Article ID: 1000-324X(2011)10-1116-05 **DOI:** 10.3724/SP.J.1077.2011.11152

Effect of Ba-doping on the Structural, Grain Orientation and Thermionic Emission Properties of Hexaboride GdB_6

BAO Li-Hong, ZHANG Jiu-Xing, ZHOU Shen-Lin

(Key Laboratory of Advanced Functional Materials, Ministry of Education, College of Materials Science and Engineering, Beijing University of Technology, Beijing 100124,China)

Abstract: The polycrystalline rare-earth hexaborides $(Ba_xGd_{1-x})B_6$ (x = 0, 0.2, 0.4, 0.8) were prepared by the reactive spark plasma sintering (SPS) method using mixed powder of BaH_2, GdH_2 and B. The effects of Ba doping content on the crystal structure, the grain orientation and the thermionic emission properties of the GdB_6 were investigated by X-ray diffraction, electron backscattered diffraction and emission current measurements. It is found that all the sintered samples exhibit high densification (> 97%) and high value of Vickers hardness (2070 kg/mm^2). The maximum thermionic emission current density of GdB_6 is 11 A/cm^2 at a cathode temperature of 1873 K, which is much higher than that of traditional method. With the increase of Ba content, the thermionic emission current density decreases from 11 A/cm^2 to 2.25 A/cm^2 at 1873 K.

Key words: rare-earth hexaborides; spark plasma sintering; emission property; doping

Rare-earth hexaborides crystallize into the simple cubic CaB_6-type structure and they have been extensively investigated both theoretically and experimentally. Among the rare-earth hexaborides family, LaB_6[1-3] and CeB_6[4-5] as excellent thermionic electron emitters were characterized by high brightness, thermal stability, low volatility and high mechanical strength. These advantages are originated from their low work function (2.4–2.6 eV), high melting point (2510–2715℃) and covalent bond of B–B atom in crystal structure. The GdB_6[6-7] is extensively studied about its complicated magnetic transport properties, which has two magnetic phase-transition temperatures around 8 K and 15 K. Another important feature of GdB_6 is that it has the lowest work function (about 2.05 eV)[8] in the rare-earth hexaborides. Zhang *et al* [9] have prepared the GdB_6 single crystalline nanowires by the chemical vapor deposition method and measured the filed emission properties. However, the thermionic emission properties of GdB_6 have very rarely been reported in the literature so far. In addition, it is difficult to prepare the high density polycrystalline bulks of GdB_6[10] by the traditional solid-phase sintering method, owing to the powder characterization of high plastic yield stress. Therefore, there are great research prospects for full densification of bulk GdB_6, especially regarding to its excellent thermionic emission or field emission properties.

Schmidt *et al*[11] reported that the $La_{0.3}Pr_{0.7}B_6$ and $La_{0.3}Nd_{0.7}B_6$ show a lower effective work function than LaB_6 by doping La element to PrB_6 and NdB_6. Therefore, appropriate ratio of doping rare-earth element[12-13] can significantly improve the emission property. Based on above studies, it can be inferred that the full densification and the appropriate ratio of dopings are two important factors for obtaining reproducible and improved properties.

In the present work, the high density polycrystalline GdB_6 is fabricated by the spark plasma reactive liquid-phase sintering (SPS) method and the Ba-doping effects on structural, grain orientation and thermionic emission properties are investigated.

1 Experimental

The BaH_2 and GdH_2 nanopowder were prepared in a mixed gas of hydrogen and argon using the raw material Barium (99.96% purity) and Gadolinium (99.9% purity). The fixed molar ratios of amorphous boron powder (99.9% purity, 10 μm), BaH_2 and GdH_2 nanopowders were mixed in an agate mortar. The mixture was placed into a graphite die with inner diameter of 20 mm for liquid-phase SPS processing using a sumimoto SPS-3.20MK-V sinter-

Received date: 2011-03-14; **Modified date:** 2011-04-18; **Published online:** 2011-05-20
Foundation item: National Natural Science Foundation of China (50871002)
Biography: BAO Li-Hong (1983−), male, candidate of PhD. E-mail: baolihong_10@yahoo.com.cn
Corresponding author: ZHANG Jiu-Xing, professor. E-mail: zjiuxing@bjut.edu.cn

ing system. The following conditions are applied for the SPS sintering: axial mechanical pressure of 50 MPa, heating rate of 110℃/min, sintering temperature of 1450–1500℃ with holding for 5 min. The phase identification and the compositions of the $(Ba_xGd_{1-x})B_6$ were examined by X-ray diffraction (CuKα radiation, Bruker D8) and X-ray fluorescence (XRF: Magix PW2403). The powder morphology was characterized using transmission electron microscope (TEM: JEM-2010) and the electron backscattered diffraction (EBSD) investigation was carried out in a FEINANO 200 scanning electron microscope incorporating an EDAX TSL OIM5.2 system. The densities of all sintered bulks were measured by using the Archimedes method and then compared with their theoretical densities. Testing of the electron emission properties was carried out at the University of Electronic Science and Technology of China. The emission area of the cathode was 1 mm^2 for thermionic emission measurement. The Vickers hardness was measured by using MICROHARDNESS TESTER FM-700 under a load of 5 N.

2　Results and discussion

2.1　Morphology of the GdH_2 and BaH_2 nanopowder

Figure 1 shows the TEM images of the GdH_2 and BaH_2 nanopowder fabricated by evaporation-condensation method. The primary particles of both GdH_2 and BaH_2 are nearly spherical morphology, with a size of about 20–30 nm of GdH_2, 50–80 nm of BaH_2 except for a small number of aggregation. Compared with coarse powder, the nanopowder is featured by the high diffusion coefficient, the high surface energy and the low melting point, which are beneficial for GdH_2 and BaH_2 reacting with boron to form hexaborides at a lower sintering temperature.

2.2　Phase and crystal structure identification of $(Ba_xGd_{1-x})B_6$ bulks

Figure 2 shows the XRD patterns of the polycrystalline $(Ba_xGd_{1-x})B_6$ (x= 0, 0.2, 0.4, 0.8) bulks sintered at different temperatures. Figure 2(a) indicates that without Ba-doping content, the GdB_6 bulks compose of a large amount of GdB_6 main phase and the GdB_4 impurity phase with P4/mbm symmetry, after sintered at 1450℃ under 50 MPa. From Fig. 2(b), it can be found that when the sintering temperature increases to 1500℃, the single phase of GdB_6 is obtained without GdB_4 impurity phase. This indicates that the reaction temperature of B and Gd to form GdB_6 is 1500℃ under the sintering pressure of 50 MPa. Furthermore, the phase compositions of all sintered samples with various Barium dopings are composed of single phase with space group Pm3m, which indicates that the Ba atoms randomly substitute the Gd atoms shown in Fig. 2(b). The refined lattice parameters obtained by fitting the measured XRD patterns with standard structure models are given in Table 1. It can be clearly seen that the Ba element doping leads to an increase of lattice expansion, since the substitute atom radius of Ba (0.278 nm) is larger than that of Gd (0.254 nm). The chemical purity of all sintered samples maintains the value of above 99.9%

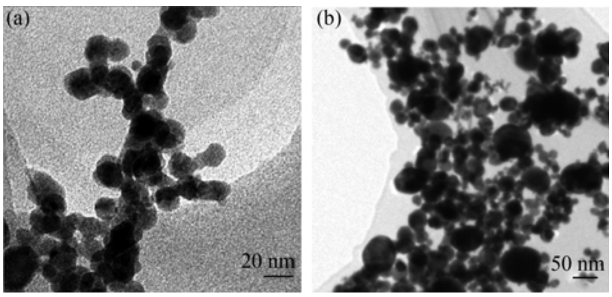

Fig. 1　TEM images of the GdH_2 (a) and BaH_2 (b) nanopowder

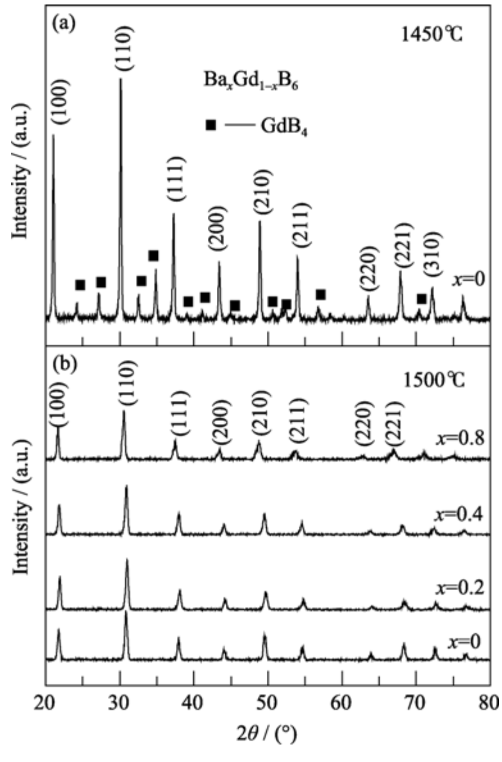

Fig. 2　XRD patterns of GdB_6 sintered at 1450℃ under 50MPa(a) and $(Ba_xGd_{1-x})B_6$ (x= 0, 0.2, 0.4, 0.8) sintered at 1500℃ under 50MPa (b)

Table 1　The partial properties of $(Ba_xGd_{1-x})B_6$ bulks

$(Ba_xGd_{1-x})B_6$	Purity / %	Lattice constant / nm	Relative density / %	Vickers hardness/ $(kg{\cdot}mm^{-2})$
GdB_6	99.92	0.4099	97. 5	2091
$Ba_{0.2}Gd_{0.8}B_6$	99.91	0.4131	98.1	1985
$Ba_{0.4}Gd_{0.6}B_6$	99.94	0.4157	97.3	2006
$Ba_{0.8}Gd_{0.2}B_6$	99.93	0.4221	99.0	2070

measured by XRF shown in Table 1.

2.3 Mechanical property of $(Ba_xGd_{1-x})B_6$ bulks

The relative density of the $(Ba_xGd_{1-x})B_6$ (x=0, 0.2, 0.4, 0.8) bulks as a function of doping content x is listed in Table 1. It can be seen that the high relative density (> 97%) of $(Ba_xGd_{1-x})B_6$ ceramics can be achieved by SPS method. It was reported that the relative density of GdB_6 bulk obtained by traditional sintering of GdB_6 powders is about 80%[10], indicating this approach is ineffective to full densification. However, in this work, the typical liquid reactive SPS mechanism lead to the promoting the consolidation procedure. When the sintering temperature is in the range of 729–883℃, there is a dehydrogenation reaction[14-15] between BaH_2 and GdH_2, and then they form the liquid phase Ba, Gd nanopowder and H_2 gas, respectively. When the sintering temperature increases up to 1500℃, the liquid phase of Ba and Gd soak and react with boron powder to form the single phase hexaboride shown in Fig. 2(b). The melting point of Ba and Gd is 725℃ and 1313℃, respectively. Obviously, the emergence of liquid phase has promoted the sintering by enhancing the rate of mass transport of solid phase boron and has induced to grain rearrangements, which are beneficial for improving the densification. It can also be found from Table 1 that the Vickers hardness of all sintered bulks maintains the higher value, the maximum reaches 2070 kg/mm^2.

2.4 Electron backscatter diffraction (EBSD) analysis of grain orientation

Figure 3 shows the EBSD orientation maps of polished $(Ba_xGd_{1-x})B_6$ (x=0, 0.4, 0.8) bulks. Different color regions represent the crystallographic orientation according to the inverse pole figure (IPF) shown in footer. The average grain size is in the range of 1 μm to 3 μm except for a small quantity of large grains. This result well corresponds with the fracture surface observation of SEM. Figure 4 shows the corresponding normal direction (*i.e.* parallel to the axial direction of sintered sample) inverse pole figures, where the color depth indicates the pole area density. It is seen that the maximum texture intensity of GdB_6 mainly composes of (111) fiber texture, the $Ba_{0.4}Gd_{0.6}B_6$ composes of (110) fiber texture and $Ba_{0.8}Gd_{0.2}B_6$ composes of (100) fiber texture. According to previous investigations[16-17], the work functions (Φ) of hexaborides are related to its surface: the order of Φ for the different surfaces was $\Phi_{(310)}<\Phi_{(210)}<\Phi_{(100)}<\Phi_{(110)}<\Phi_{(111)}<\Phi_{(211)}$. Therefore, it is predicted that the $(Ba_xGd_{1-x})B_6$ bulks with fiber texture will have superior emission properties.

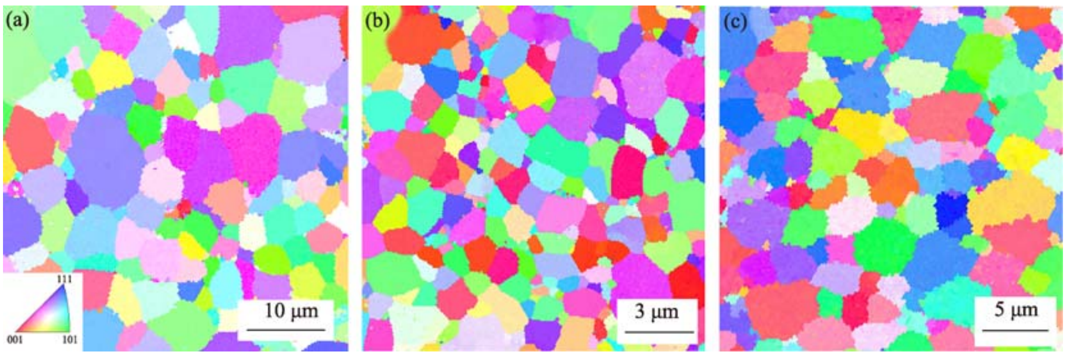

Fig. 3 The orientation maps for normal direction of $(Ba_xGd_{1-x})B_6$ bulk
(a) x=0; (b) x= 0.4; (c) x=0.8

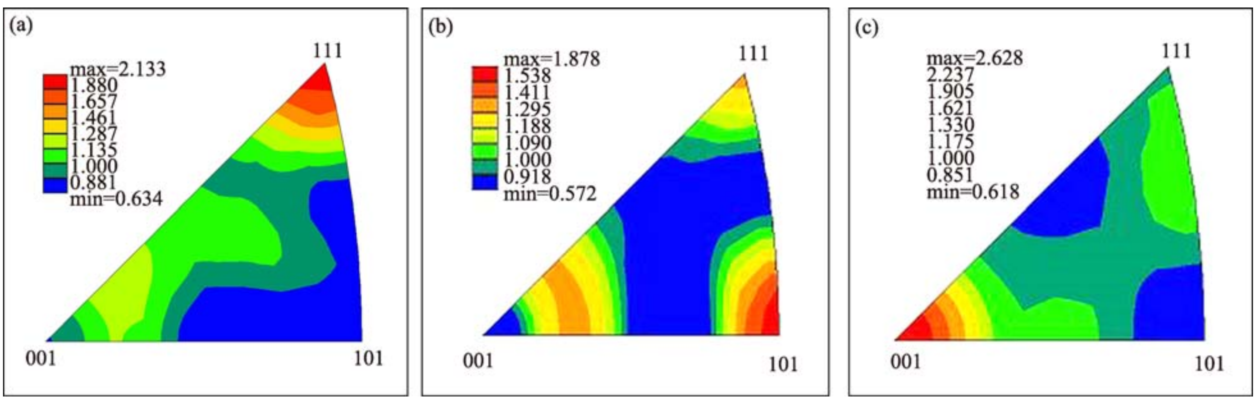

Fig. 4 The inverse pole figures of $(Ba_xGd_{1-x})B_6$ bulk
(a) x=0; (b) x=0.4; (c) x=0.8

2.5 Thermionic emission properties of $(Ba_xGd_{1-x})B_6$ (*x* = 0, 0.2, 0.4, 0.8)

The thermionic emission current density of $(Ba_xGd_{1-x})B_6$ (x=0, 0.2, 0.6, 0.8) was measured with voltages up to 1000 V at various cathode temperatures from 1673 K to 1873 K. The results are shown in Fig. 5. It can be seen from Fig. 5(a) that with the increase of applied voltage, the maximum emission current density of GdB_6 is 0.37 A/cm^2 at 1673 K. When the measuring temperature increases to 1773 K and 1873 K, the maximum values of emission current density are 2.76 A/cm^2 and 11 A/cm^2, respectively. Storms, *et al*[10] reported the emission current density of GdB_6 prepared by traditional hot-pressing method is only 0.00042 A/cm^2 with the voltage of 1400 V at 1700 K, which is much smaller than that of this work. The improvement of emission current density is attributed to the high densification and grain preferred orientation by SPS method. Figure 5(b) shows the emission current density of the doping content with x=0.2, 0.4 and 0.8 measured at 1873K. It can be seen that when the Ba doping content is 20at% and 40at%, the maximum emission current density are 0.8 A/cm^2 and 1.2 A/cm^2, respectively. Furthermore, when the doping content increases to 80at%, its peak value of emission current density increases to 2.25 A/cm^2. However, comparing the emission current densities of GdB_6 with the Ba-doping hexaborides, the Ba element rapidly decreases the emission current density, which is out of expectation. In order to further study the reason of Ba-doping lead to the reduction of emission current density, we have measured the electrical resistivity of $(Ba_xGd_{1-x})B_6$ bulks with x=0, 0.4 and 0.8. The results show that the electrical resistivity of $Ba_{0.4}Gd_{0.6}B_6$ and $Ba_{0.8}Gd_{0.2}B_6$ are 494 and 121 μΩ·cm, which are higher than that of 90 μΩ·cm of GdB_6. Therefore, it can be inferred that the increase of electrical resistivity may lead to the decrease of emission current density.

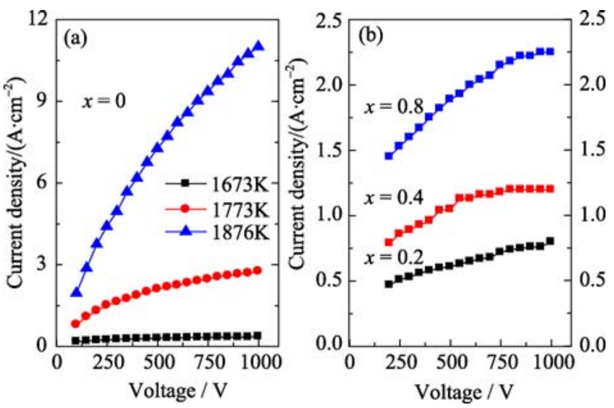

Fig. 5 $(Ba_xGd_{1-x})B_6$ emission current density dependence on the different doping contents
(a) x = 0; (b) x = 0.2, x = 0.4 and x = 0.8 measured at 1873K

3 Conclusions

The high densified polycrystalline $(Ba_xGd_{1-x})B_6$ were prepared by the *in situ* SPS sintering using the GdH_2, BaH_2 and B powder in an oxygen free system. The typical reactive liquid-phase SPS mechanism is useful to attain grain preferred orientation and excellent mechanical properties. The maximum thermionic emission current density of GdB_6 is 11 A/cm^2 at a cathode temperature of 1873 K, which is much higher than that prepared by traditional method. With the increase of Ba content, the thermionic emission current density decreases linearly. Thus, it can be concluded that the SPS technique represents a suitable method to synthesize high dense rare-earth hexaborides with excellent properties.

References:

[1] Nishitani R, Aono M, TanaKa T, *et al.* Surface states on the LaB_6(100), (110) and (111) clean surfaces studied by angle-resolved UPS. *Surf. Sci.*, 1980, **95(2/3):** 341–358.

[2] Goebel D M, Watkins R M, Jameson K K. LaB_6 hollow cathodes for ion and hall thrusters. *J. Propul. Powder,* 2007, **23(3):** 552–558.

[3] Choi Y W, Cho C, Choi Y S, *et al*. Development of a 30 kW plasma gun system with a long lifetime. *IEEE Trans. Plasma Sci.,* 2008, **36(5):** 2765–2769.

[4] Swanson L W, McNeely D R. Work functions of the (001) face of the hexaborides of Ba, La, Ce and Sm. *Surf. Sci.*, 1979, **83(1):** 11–28.

[5] Zhou S L, Zhang J X, D. M. Liu, *et al*. Properties of CeB_6 cathode fabricated by spark plasma reactive liquid phase sintering method. *J. Inorg. Mater*., 2009, **24(4):** 793–797.

[6] Reiffers M, Sebek J, Santava E, *et al.* Thermal hysteresis of the phase-transition temperature of single-crystal GdB_6. *Phys. Stat. Sol. (b),* 2006, **243(1):** 313–316.

[7] Luca S E, Amara M, Galera R M, *et al*. Neutron differaction studies on GdB_6 and TbB_6 powders. *Physica B*, 2004, **350:** e39–e42.

[8] Cheng H, Jiang J P. Cathode Electronics. Northwest Institute of Telecommunication Publishing House, 1986: 85–86.

[9] Zhang H, Zhang Q, Zhao G P, *et al.* Single-crystalline GdB_6 nanowire field emiters. *J. Am. Chem. Soc.,* 2005, **127(38):** 13120–13121.

[10] Storms E K, Mueller B A. Thermionic emission and atom vaporization of the Gd-B system. *J. Appl. Phys*., 1981, **52(4):** 2966–2969.

[11] Schmidt P H, Joy D C. Low work function electron emitter hex-

aborides. *J. Vac. Sci. Technol.,* 1978,**15(6):** 1809−1810.

[12] Ma R G, Liu D M, Zhou S L, *et al*. Fabrication and emission property of polycrystalline $La_{0.4}Pr_{0.6}B_6$ bulk prepared by spark plasma sintering. *J. Inorg. Mater.,* 2010, **25(7):** 1−5.

[13] Liu S P, Yang Q S, Chen W P, *et al*. Development of RE multiple boride $(La_{0.55}Ba_{0.45})B_6$ and $(La_{0.4}Eu_{0.6})B_6$ cathode materials. *Rare Metals and Cemented Carbides.,* 2006, **34(3):** 8−11.

[14] Zhou S L, Zhang J X, Liu D M, *et al*. Fabrication and charact erization of high—purity nanostructured bulk LaB_6 polycrystal cathode material. *J. Inorg. Mater*., 2008, **23(6):** 1199−1204.

[15] Zhou S L, Zhang J X, Liu D M, *et al*. Synthesis and properties of nanostructured dense LaB_6 cathodes by arc plasma and reactive spark plasma sintering. *Acta Mater.,* 2010, **58(15):** 4978−4985.

[16] Uijttewaal M A, DeWijs G A, Groot R A. Ab initio and work function and surface energy anisotropy of LaB_6. *J. Phys. Chem. B*, 2006, **110(37):** 18459−18465.

[17] Gesley M, Swanson L W. A determination of the low work function planes of LaB_6. *Surface Science,* 1984, **146(2/3):** 583−599.

Ba 掺杂对稀土硼化物 GdB_6 结构, 晶粒取向和热发射性能的影响

包黎红, 张久兴, 周身林

(北京工业大学 材料学院新型功能材料教育部重点实验室, 北京 100124)

摘 要: 采用反应放电等离子烧结技术, 以 BaH_2, GdH_2 纳米粉和 B 粉为原料, 成功制备了多晶稀土硼化物$(Ba_xGd_{1-x})B_6$ (x=0, 0.2, 0.4, 0.8). 采用 XRD、EBSD 技术研究了掺杂元素 Ba 对 GdB_6 晶体结构及晶粒取向的影响, 并测量不同温度下的热发射性能. 结果表明, 所有烧结样品与传统烧结方法相比, 具有高致密度(>97%)和很高的维氏硬度(2070 kg/mm^2). GdB_6 在 1873 K 时, 最大发射电流密度为 11 A/cm^2, 该值远高于传统方法制备的电流密度值. 随着 Ba 含量的增加, 发射电流密度从 11 A/cm^2 减小到 2.25 A/cm^2.

关 键 词: 稀土硼化物; 放电等离子烧结; 发射性能; 掺杂

中图分类号: TB34 **文献标识码:** A

勘 误

本刊发表论文《电致变色纳米氧化镍薄膜的溶胶−凝胶法制备与表征》(2004, 19(6): 1391-1396), 作者单位“3. 合成工业大学, 合肥 230009”, 现更正为“3. 合肥工业大学, 合肥 230009”.

特此勘误!

《无机材料学报》编辑部

2011-09-09